symmetry

MDPI

Article

Spin Sum Rule of the Nucleon in the QCD Instanton Vacuum

Ismail Zahed

Center for Nuclear Theory, Department of Physics and Astronomy, Stony Brook University, Stony Brook, NY 11794-3800, USA; ismail.zahed@stonybrook.edu

Abstract: We briefly review some essential aspects of the QCD instanton vacuum in relation to the quantum breaking of conformal symmetry, the spontaneous breaking of chiral symmetry, and the axial U(1) anomaly. The anomaly causes the intrinsic nucleon spin to transmute to the vacuum topological charge by quantum tunneling. We use Ji′*s* invariant spin decomposition to discuss the spin budget of the nucleon as a quark–diquark state in the QCD instanton vacuum. A measure of the intrinsic quark spin of the nucleon is a measure of the quenched topological susceptibility of the QCD instanton vacuum.

Keywords: QCD vacuum; axial anomaly; spin sum rule

Citation: Zahed, I. Spin Sum Rule of the Nucleon in the QCD Instanton Vacuum. *Symmetry* **2022**, *14*, 932. https://doi.org/10.3390/sym14050932

Academic Editor: Dubravko Klabučar

Received: 13 April 2022
Accepted: 2 May 2022
Published: 4 May 2022

1. Introduction

The nucleon is a spin-$\frac{1}{2}$ object composed of quarks and gluons. However, how does its spin arise from its constituents? Historically, this question was answered in the context of the constituent quark model: the nucleon is composed of three weakly interacting constituent quarks, and the nucleon spin arises from the composition of their spin. The gluons only help bind the quarks.

This reductionist view of the nucleon was challenged by the EMC experiment [1]. More recently, a double spin asymmetry analysis by the COMPASS collaboration has shown that only 30–40% of the nucleon intrinsic spin is carried by the quarks [2]. These initially surprising results led to a flurry of activities both experimentally and theoretically, with most wondering about where the spin was [3].

Dedicated lattice simulations have by now provided the natural answer [4,5]: the proton spin is the sum of the spin and the angular momentum of its partonic constituents, with the contributions varying with the resolution. For a recent review of both the experimental status and the lattice measurements of the proton spin, we refer the reader to [6] (and references therein).

However, the lattice answer, while quantitative, does not provide the physical insights into the mechanism(s) underlying this spin composition. For that, we need a better understanding of the non-perturbative aspects of the gauge configurations in the QCD vacuum state and how they affect the spin composition of hadrons.

The QCD vacuum, as a liquid of instantons and anti-instantons [7–9], offers such an understanding that is rooted in QCD. The purpose of this article is to show how the intrinsic quark spin of the nucleon in this liquid is regulated by the vacuum topological fluctuations and why the real gluon angular momentum contribution to the nucleon spin is naturally small at the resolution fixed by the mean instanton size.

In Section 2 we review some aspects of the QCD instanton liquid in relation to the quantum breaking of conformal symmetry and the spontaneous breaking of chiral symmetry. We briefly address the role of thin center P-vortices. The quark and gluon composition of the nucleon spin using Ji′*s* decomposition [10] and the role of the U(1) axial anomaly are discussed in Section 3. In Appendix A, we suggest that the measure of the quark intrinsic spin in the nucleon is a measure of the quenched topological susceptibility of the QCD instanton vacuum as a topological liquid. Our conclusions are discussed in Section 4.

2. Yang-Mills Vacuum

The chief aspects of the Yang-Mills vacuum is its quantum breaking of conformal symmetry and the ensuing spontaneous breaking of chiral symmetry. The main gauge fields at the origin of these two fundamental mechanisms were made visible in the stunning pictures developed by Leinweber and his collaborators [11–13], who used cooling and/or projection techniques of lattice gauge configurations, as illustrated in Figure 1. The numerical pictures reveal a smooth landscape made of instantons and anti-instantons threaded by thin center vortices or Z_3-fluxed strings, which span world-sheet surfaces in four dimensions.

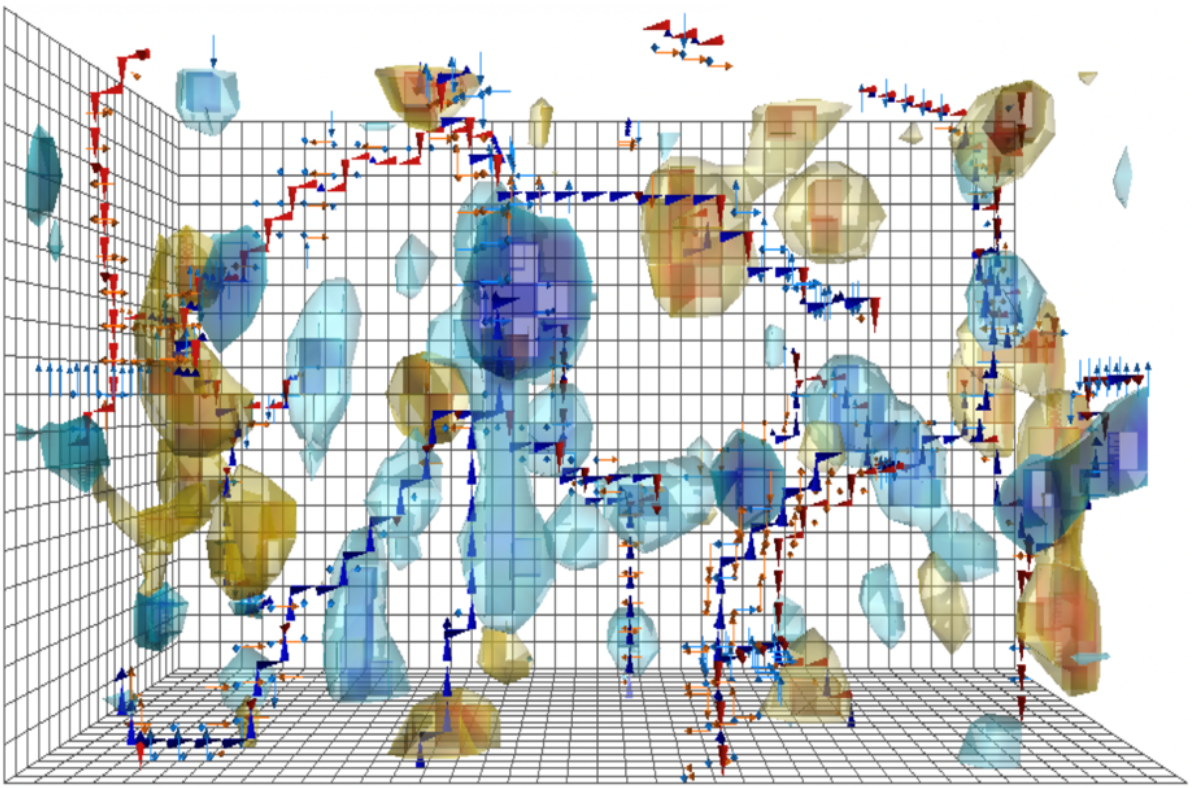

Figure 1. Configurations of instantons (yellow) and anti-instantons (blue) in the cooled Yang-Mills vacuum after center projection, threaded by center P-vortices [11,12]. They constitute the primordial gluon epoxy (hard glue) at the origin of the light hadron masses. The center P-vortices are responsible for the confinement (see text).

2.1. Primordial Epoxy

The size distribution of the instantons and anti-instantons in the Yang-Mills vacuum is well-captured semi-empirically by [7–9]:

$$dn(\rho) \sim \frac{d\rho}{\rho^5} \left(\rho \Lambda_{QCD}\right)^b e^{-\#\rho^2/R^2} \tag{1}$$

with $b = 11N_c/3 - 2N_f/3$ (one loop). The small size distribution follows from the conformal nature of the instanton moduli and the perturbation theory. The large size distribution is non-perturbative, but the mean separation of the instantons (anti-instantons) is cut off by R in the vacuum. Remarkably, the mean density or tunneling rate and size were predicted long ago by Shuryak [14].

$$n_{I+\bar{I}} = \frac{\bar{N}}{V} \equiv \frac{1}{R^4} \approx \frac{1}{\text{fm}^4} \qquad \frac{\bar{\rho}}{R} \approx \frac{1}{3} \tag{2}$$

The hadronic spectrum and correlations following from the cooling configurations in Figure 1 are similar to those before cooling—an observation that is supported by earlier

studies [8,15]. The dimensionfull parameters (2) combine in the dimensionless parameter $\kappa \equiv \pi^2 \bar{\rho}^4 n_{I+\bar{I}} \approx 0.1$, which is a measure of the diluteness of the instanton–anti-instanton ensemble in the QCD vacuum. It is this diluteness that allows for an analytical analysis of the vacuum in Figure 1 with the use of the semi-classical expansion in gauge theory and many-body physics.

The quantum breaking of conformal symmetry is best captured by the anomalous part of the trace of the energy-momentum tensor.

$$T^{\mu}_{\mu} \approx -\frac{b}{32\pi^2} F^a_{\mu\nu} F^{a\mu\nu} + m\bar{\psi}\psi \tag{3}$$

Throughout this paper, we will use the rescaling $gF \to F$ for operators in the instanton or anti-instanton gauge fields. In the QCD instanton vacuum, the gluon operator $F^2/(32\pi^2) \to (N_+ + N_-)/V = N/V$ counts the number of instantons plus anti-instantons in the 4-volume V, while $F\tilde{F}/32\pi^2 \to (N_+ - N_-)/V = \tilde{N}/V$ counts their difference in the 4-volume V. In the canonical ensemble with zero theta angle, the former is fixed by the mean instanton density, with $N_\pm/V \to \bar{N}/2V$ and $\tilde{N} = 0$. Therefore, we have the following:

$$\left\langle T^{\mu}_{\mu} \right\rangle \approx -b\, n_{I+\bar{I}} + m\langle\bar{\psi}\psi\rangle \approx -b\left(\frac{\bar{N}}{V}\right)\left(1 + \mathcal{O}(mR)\right) \approx -10\,\mathrm{fm}^{-4} \tag{4}$$

thus setting the scale of all hadrons. The explicit chiral breaking contribution is small, with $mR \approx (8\,\mathrm{MeV})(1\,\mathrm{fm}) \approx 1/25$ at the soft renormalization scale $\bar{\rho} \approx 0.3$ fm. The gluon condensate $\langle F^2 \rangle$, which is positive, is referred to as the primordial epoxy or hard glue (a term coined by the late Gerry Brown) at the origin of the hadronic mass in the Universe. The gluon epoxy in the nucleon is the quantum anomalous energy in the nucleon discussed recently in [16].

In Figure 1, the instanton number $N = N_+ + N_-$ and the topological charge $\tilde{N} = N_+ - N_-$ fluctuate, with a universal measure fixed by low-energy theorems for N (all moments) [17] and a topological susceptibility for $\tilde{N}$ (variance), that is [9,18,19]:

$$\mathbb{Q}(N_+, N_-) = \left[e^{\frac{bN}{4}} \left(\frac{\bar{N}}{N}\right)^{\frac{bN}{4}}\right]\left[\frac{1}{(2\pi\chi_{\mathbb{Q}})^{\frac{1}{2}}} e^{-\frac{\tilde{N}^2}{2\chi_{\mathbb{Q}}}}\right] \tag{5}$$

The leading moments are respectively

$$\frac{\langle (N-\bar{N})^2 \rangle_{\mathbb{Q}}}{\bar{N}} = \frac{4}{b} \qquad \langle \tilde{N}^2 \rangle_{\mathbb{Q}} = \chi_{\mathbb{Q}} \tag{6}$$

The variance in N is the vacuum compressibility, which is seen to vanish in the large N_c limit (the vacuum crystallizes). The variance in $\tilde{N}$ is the following topological susceptibility:

$$\frac{\chi_{\mathbb{Q}}}{V} = \frac{\langle \tilde{N}^2 \rangle_{\mathbb{Q}}}{V} = \int d^4x \left\langle \frac{1}{32\pi^2} F\tilde{F}(x)\, \frac{1}{32\pi^2} F\tilde{F}(0) \right\rangle_{\mathbb{Q}} \tag{7}$$

In quenched QCD, (7) is given by the Witten–Veneziano formula [20,21]:

$$\frac{\chi_{\mathbb{Q}}}{V} = \frac{\langle \tilde{N}^2 \rangle_{\mathbb{Q}}}{V} = \frac{f_\pi^2 M_1^2}{2N_f} \tag{8}$$

with M_1 being the quenched singlet mass:

$$M_1^2 = m_{\eta'}^2 + m_\eta^2 - 2m_K^2 \tag{9}$$

and with (8)–(32) holding in the QCD instanton vacuum [7–9]. In the unquenched QCD instanton vacuum, (8) is very sensitive to the presence of light quarks with the substitution $M_1^2 \to m_\pi^2$ (see below) and vanishes in the chiral limit [18,19].

2.2. Zero Modes

When a light quark crosses a tunneling configuration, it develops a zero mode that is single handed [22], an amazing phenomenon protected by topology and the Atiyah–Singer theorem. It is the delocalization of these zero modes and their interactions that is at the origin of the spontaneous breaking of chiral symmetry and the emergence of the light hadronic spectrum. Remarkably, this topological mechanism for mass generation leaves behind a distinct fingerprint: universal conductance-like fluctuations in the quark spectrum, predicted by the random matrix theory [23] and confirmed by lattice simulations [24].

In Figure 2, we show how a light up-quark helicity in a zero mode is flipped when crossing an instanton (left) or anti-instanton (right). In the zero mode, the quark spin $\vec{\sigma}$ is locked to the color $\vec{\tau}$ in a hedgehog-like configuration with $\vec{\sigma} + \vec{\tau} = \vec{0}$. This flipping is captured by the 't Hooft vertex for a single quark flavor [22]. More specifically, the LSZ-reduced forward scattering matrix for the zero mode in Figure 2 is in the Euclidean signature below:

$$n_I \left\langle u_R^\dagger(p) p \left[\sqrt{2}\varphi'(p)\hat{p}\epsilon U\right] \frac{1}{m} \left[\sqrt{2}\varphi'(p) U^\dagger \epsilon \hat{p}\right] p u_L(p) \right\rangle_U + (I, L) \leftrightarrow (\bar{I}, R) \tag{10}$$

with the Weyl notation subsumed ($p = p_\mu \sigma_\mu$), and the normalized quark zero mode as follows:

$$\psi_{iI}^\alpha(p) = \sqrt{2}\varphi'(p)(\hat{p}\epsilon U)_i^\alpha \equiv \sqrt{2}\left[\pi\rho^2\Big(I_0K_0(z) - I_1K_1(z)\Big)'_{z=\rho p/2}\right](\hat{p}\epsilon U)_i^\alpha \tag{11}$$

Here, the matrix element $(\epsilon U)_a^i = \epsilon_b^i U_a^b$ carries spin-i and color-a, with ϵ_b^i being a real anti-symmetric tensor (hedgehog in spin color) and U an $SU(N_c)$ valued color matrix. The averaging in (11) is carried over U, while (10) can be recast in the following form:

$$M_u(p)\left(\frac{N}{\bar{N}}\, u^\dagger(p)u(p) - \frac{\tilde{N}}{\bar{N}}\, u^\dagger(p)\gamma^5 u(p)\right) \to u^\dagger(p)\left[M_u(p)\left(1 - \frac{\tilde{N}}{\bar{N}}\gamma^5\right)\right]u(p) \tag{12}$$

with the running constituent quark mass [25,26] ($\tilde{\kappa} = \kappa/(2\pi^2 N_c)$):

$$M_u(p) = \tilde{\kappa}\frac{|p\varphi'(p)|^2}{m\rho^4} \to \frac{\sqrt{\tilde{\kappa}}}{\sqrt{2}\rho^2}\frac{|p\varphi'(p)|^2}{||q\varphi'^2||} \tag{13}$$

The singular $1/m$ effect is removed by disordering, with $M_u(0) = 383 \pm 39$ MeV [26], which is comparable to the numerical result $M_u(0) \approx 300$ MeV [8,27]. In the QCD instanton vacuum, the running quark mass is fixed by the same scale as the gluon condensate, or $M_u(0) \approx 1/R$ since $\bar{\rho} \approx R/3$, with the size distribution (1) still controlled by R. This ensures the renormalization group invariance of all mass scales.

The emergent quark mass (13) in the QCD instanton vacuum may remind us of the constituent quark mass from the Nambu–Jona-Lasinio (NJL) model [28,29] (and references therein). However, it is important to stress that the latter is a pre-QCD model, while the former is rooted in QCD and is now supported by even numerical QCD lattice pictures, as in Figure 1. The canonical NJL model, although useful, does not explain the vacuum gluon condensate, the running quark mass, the η' mass (unless modified), and the universal spectral conductance fluctuations [23], among other things. For completeness, we note the non-topological approach to the hadronic mass scale in [30] (and references therein), where a running quark mass also emerges by re-summing gluon rainbow diagrams.

Figure 2. Quark spin (helicity) in zero mode being traded in and out of an instanton (**left**) and anti-instanton (**right**), at the origin of the mixing of the quark spin and the topological charge in the QCD instanton vacuum (see text).

2.3. Center P-Vortices

The thin and long center-projected P-vortices in Figure 1 that survive the moderate cooling procedure (about seven to eight cooling sweeps) [11,12] are responsible for the disordering of the large Wilson loops, and therefore confinement, at larger distances. These thin vortices, with a size given by a lattice length, are generated on the lattice as follows: (1) Each of the links in a lattice plaquette is projected onto the center of the gauge group Z_{N_c}; (2) The product of the centers around a plaquette is an element of the center in the dual lattice; (3) By extending these projections to all lattice plaquettes, the initial gauge configuration is center-projected; (4) The center-projected P-vortex is the closed string threading these Z_{N_c} flux lines on the dual lattice. A Wilson loop winding around this P-vortex counts the Z_{N_c} fluxes. A continuum description of these thin P-vortices and their subtleties is discussed in [31].

The instantons and anti-instantons only contribute to the logarithmic growth of the potential between heavy quarks [32], which is not enough. Any center P-vortex that links with a large Wilson loop will produce a Z_{N_c} flux. A random collection of these fluxes by the Wilson loop can be reduced to a binomial sum that exponentiates to an area law in the thermodynamical limit. The emergent string tension $\sigma_T = N_V/\sqrt{V}$ is fixed by the planar density of center P-vortices [33]. Since $\sigma_T = 1/(2\pi l_s^2)$ with the string length $l_s \approx 0.2$ fm, this translates to a center P-vortex planar density of about $N_V/\sqrt{V} \approx 4/\text{fm}^2 \approx 4/R^2$. Note that all topological charges in Figure 1 are anchored to the branching points along the center P-vortices. How the P-vortex planar density relates to the mean instanton density is still an important open question.

While the center vortices are important for enforcing confinement at long distances, Figure 1 shows that they are on average decoupled from the inhomogeneous and strong topological fields. Moreover, their field strength in the vicinity of these topological fields is about $\sigma_T\bar{\rho} \approx 0.3\,\text{GeV}$, which is weaker than the typical chromo-electric or chromo-magnetic field in the instanton center $\sqrt{E} = \sqrt{B} \approx 2.5/\bar{\rho} \approx 1.5\,\text{GeV}$. This suggests that the quantum breaking of conformal symmetry and the spontaneous breaking of chiral symmetry, both for the vacuum and the low-lying hadronic excitations, are mostly driven by the strong and inhomogeneous topological gauge fields.

Perhaps, where confinement becomes important is for the orbitally excited hadronic excitations, as the underlying quark sources follow wider world lines that are likely to link more frequently to the long and weaker center P-vortices. This point can be tested numerically. Furthermore, the branching points in these long vortices anchor the topological charges, hinting at their stability under moderate cooling. Clearly, too much cooling that removes the topological charges will also remove the long center P-vortices with the disappearance of both the string tension and the chiral condensate. This remarkable geometrical relationship between the long vortices and the topological charges may explain why the deconfinement transition and the chiral symmetry restoration temperature are so close in QCD [34].

We will not further pursue these and other challenging questions here. Instead, we will mostly focus on the topological gauge fields, which are essentially composing the instanton liquid we presented above.

3. Ji Spin Sum Rule

A frame-independent and gauge-invariant decomposition of the nucleon spin was suggested by Ji in [10]. In that study, the nucleon spin is the sum of the intrinsic quark spin $\vec{\Sigma}/2$, the quark orbital angular momentum $\vec{L}_Q$, and the gluon angular momentum $\vec{J}_G$:

$$\vec{J} = \left(\frac{1}{2}\vec{\Sigma} + \vec{L}_Q\right) + \vec{J}_G \tag{14}$$

In the Minkowski signature, the quark part is the following:

$$\vec{J}_Q = \frac{1}{2}\vec{\Sigma} + \vec{L}_Q = \int d^3x \left(\frac{1}{2}\overline{\psi}\vec{\gamma}\gamma^5\psi + \psi^\dagger(\vec{x}\times i\vec{D}[A])\psi\right) \tag{15}$$

and the gluon part is as follows:

$$\vec{J}_G = \int d^3x \left(\vec{x}\times(\vec{E}^a\times\vec{B}^a)\right) \tag{16}$$

The quark orbital and gluon angular momentum depend on the renormalization scale and scheme, but their sum does not. The quark spin is tied to the U(1) anomaly and is therefore scale-independent. The nucleon spin budget is then as follows:

$$\vec{J}_N = \frac{\langle PS|\vec{J}|PS\rangle}{\langle PS|PS\rangle} \equiv \frac{1}{2}\vec{\Sigma}^N_Q + \vec{L}^N_Q + \vec{J}^N_G \tag{17}$$

When translated to the Euclidean signature, we readily observe that at the soft renormalization scale $\bar{\rho} = 0.3$ fm, the gluonic contribution to the spin is the sum of multi-instanton contributions of the form:

$$\begin{aligned}(\vec{E}^a\times\vec{B}^a)[A] = &\sum_{I=1}^{N_\pm}(\vec{E}^a\times\vec{B}^a)[A_I(\xi_I)] + \sum_{I\neq J}^{N_\pm}(\vec{E}^a\times\vec{B}^a)[A_I(\xi_I),A_J(\xi_I)] + \ldots\\ = &\sum_{I\neq J}^{N_\pm}(\vec{E}^a\times\vec{B}^a)[A_I(\xi_I),A_J(\xi_I)] + \ldots\end{aligned} \tag{18}$$

The instantons and anti-instantons are self-dual with $\vec{E}^a[A_I] = \pm\vec{B}^a[A_I]$ for all $I = 1,\ldots N_\pm$, so the first contribution in (18) vanishes. When averaged over a measure of independent instantons and anti-instantons, the remaining contributions in (18) are down by a power of $\kappa \approx 0.1$. As a result, the gluon contribution to the angular momentum is down by κ in comparison to the quark orbital contribution, i.e., $J_G/L_Q \approx \kappa$. This will be used in the budgeting of the nucleon spin below.

3.1. U(1) Axial Anomaly

The quark intrinsic spin contribution to the nucleon is tied to the axial singlet U(1) current by the anomaly:

$$\partial_\mu\,\overline{\psi}\gamma^\mu\gamma^5\psi = \frac{N_f}{16\pi^2}F\tilde{F} + 2m\overline{\psi}i\gamma^5\psi \tag{19}$$

In the chiral limit, the fermionic spin (helicity) mixes with the bosonic topological charge of the gauge fields. This is how the intrinsic spin transmutes to the topological charge through quantum tunneling. Indeed, in a polarized nucleon state, (19) gives the following (on the left-hand side):

$$\partial_\mu\langle P'S|\overline{\psi}\gamma^\mu\gamma^5\psi|PS\rangle = \quad \Sigma^N_Q(q)\,\overline{N}_S(p')iq_\mu\gamma^\mu\gamma^5 N_S(p) \tag{20}$$

and (on the right-hand side):

$$\frac{N_f}{16\pi^2}\langle P'S|F\tilde{F}|PS\rangle + 2m\langle P'S|\overline{\psi}i\gamma^5\psi|PS\rangle = \left(\frac{N_f}{16\pi^2}A_F(q)m_N + 2mA_P(q)\right)\overline{N}_S(p')i\gamma^5 N_S(p) \quad (21)$$

with the intrinsic quark spin identification:

$$\Sigma_Q^N \equiv \Sigma_Q^N(0) = \frac{N_f}{32\pi^2}A_F(0) + \frac{m}{m_N}A_P(0) \quad (22)$$

In terms of the invariant normalization $\langle PS|PS\rangle = 2m_N(2\pi)^3\delta(0_p) = 2m_N V_3$, the quark spin is a measure of the topological charge in a polarized nucleon state [35–39]:

$$\Sigma_Q^N\overline{N}_S(p)i\gamma^5 N_S(p) = \frac{N_f V_3}{32\pi^2}\frac{\langle PS|F\tilde{F}(0)|PS\rangle}{\langle PS|PS\rangle} + \mathcal{O}\left(\frac{m}{m_N}\right) \quad (23)$$

or for a nucleon with a small velocity $\vec{v} \approx \vec{P}/m_N$ and a spin-up $s_v^{\uparrow} = \chi_{\uparrow}^{\dagger}(\vec{\sigma}\cdot\vec{v})\chi_{\uparrow}$:

$$\Sigma_Q^N \approx \frac{N_f V_3}{32\pi^2}\frac{\langle PS|F\tilde{F}(0)|PS\rangle}{s_v^{\uparrow}m_N\langle PS|PS\rangle} \quad (24)$$

3.2. Nucleon Topological Charge and Vacuum Topological Susceptibility

In the QCD instanton vacuum, the U(1) axial charge fluctuates in the grand-canonical ensemble, with the fluctuations captured by the fluctuations of the topological charge $\tilde{N} = N_+ - N_-$. The gluon contribution in (24) follows from the normalized and connected three-point function asymptotically:

$$\frac{\langle PS|F\tilde{F}(0)|PS\rangle}{\langle PS|PS\rangle} = \lim_{T\to\infty}\frac{\left\langle J_P^{\dagger}(T)F\tilde{F}(0)J_P(-T)\right\rangle_C}{\left\langle J_P^{\dagger}(T)J_P(-T)\right\rangle} \quad (25)$$

with J_P being a pertinent nucleon source. In the canonical description of the QCD instanton vacuum, $F\tilde{F}/(32\pi^2) \to \tilde{N}/V$ is a number. It factors out in the three-point correlator in (25) (numerator), and the connected correlator vanishes. The non-vanishing contribution should stem from fluctuations.

A non-vanishing contribution to the connected three-point correlator follows from the grand canonical description, where $\tilde{N}$ is allowed to fluctuate. With this in mind, it is straightforward to see that (25) is dominated by the variance of $\tilde{N}$ in the quenched vacuum [18]:

$$\frac{V}{32\pi^2}\frac{\langle PS|F\tilde{F}|PS\rangle}{\langle PS|PS\rangle} \approx \left\langle\tilde{N}^2\right\rangle_{\mathbb{Q}}\frac{\partial}{\partial\tilde{N}}\mathrm{Log}\left(\lim_{T\to\infty}\left\langle J_P^{\dagger}(T)J_P(-T)\right\rangle\right) \quad (26)$$

assuming that the skewness and curtosis of the topological charge are small. (In the unquenched case, all fluctuations in $\tilde{N}$ are vanishingly small in the chiral limit, as we note below). The result (26) was noted in [18] (see Equation (4.37)) using effective fermions, and in [19] (see Equation (92)) using effective bosons, each in the QCD instanton vacuum in the $1/N_c$ approximation. Equation (26) shows how the nucleon trades its spin with the fluctuations of the topological charge. More explicitly, (26) reads as follows:

$$\frac{V_3}{32\pi^2}\frac{\langle PS|F\tilde{F}|PS\rangle}{m_N\langle PS|PS\rangle} \approx -\langle\tilde{N}^2\rangle_{\mathbb{Q}}\left(\frac{\partial\mathrm{Log}\tilde{m}_N}{\partial\tilde{N}}\right)_{\tilde{N}=0} \quad (27)$$

since $\langle J_P^{\dagger}(T)J_P(T)\rangle$ asymptotes $e^{-2\tilde{m}_N T}$ with $\tilde{m}_N \equiv m_N(\tilde{N},\tilde{N})$, which we detail below. For completeness, we note that in [40], the same matrix element was related to the root of the slope of the topological susceptibility by an intricate argument using the renormalization group.

3.3. Intrinsic Quark Spin in the Nucleon

To evaluate (27), we use a simple description of the nucleon as a quark–scalar diquark compound, e.g., the proton with a spin up is $(uud)^{\uparrow} \approx u^{\uparrow}[ud]_0$. This schematic description captures part of the correlations in the nucleon, but not all [8]. This notwithstanding, it follows that the mixing of the proton spin with the axial charge is mostly through the unpaired u-quark. From (12), we have the following equation:

$$\tilde{m}_N \approx m_N - M_u(0) s_v^{\uparrow} \frac{\tilde{N}}{\bar{N}} \tag{28}$$

and therefore,

$$\left(\frac{\partial \mathrm{Log} \tilde{m}_N}{\partial \tilde{N}}\right)_{\tilde{N}=0} \approx -\frac{M_u(0)}{m_N} \frac{s_v^{\uparrow}}{\bar{N}} \tag{29}$$

This reasoning is similar in spirit to the one discussed in [41–43]. Inserting (29) in (27) and using (8), we obtain for (24) the following:

$$\frac{V_3}{32\pi^2} \frac{\langle PS|F\tilde{F}|PS\rangle}{m_N s_v^{\uparrow} \langle PS|PS\rangle} \approx \left(\frac{\chi_{\mathbb{Q}}}{\bar{N}}\right)\left(\frac{M_u(0)}{m_N}\right) = \frac{1}{N_f}\left(\frac{f_\pi^2 M_1^2}{2n_{I+\bar{I}}}\right)\left(\frac{M_u(0)}{m_N}\right) \tag{30}$$

Therefore, the intrinsic quark spin contribution (24) is (modulo $\mathcal{O}(m/m_N \approx 1/100)$):

$$\Sigma_Q^N \approx \left(\frac{f_\pi^2 M_1^2}{2n_{I+\bar{I}}}\right)\left(\frac{M_u(0)}{m_N}\right) \approx 0.6 \tag{31}$$

In the numerical estimate we used, $M_u \approx 300$ MeV and $m_N = 960 \pm 30$ MeV from the numerically generated QCD instanton vacuum [27], and the singlet mass $M_1 \approx 0.85\,\mathrm{GeV}$ given by the Witten–Veneziano formula in (32), or $\chi_{\mathbb{Q}}/\bar{N} \approx 1.95/N_f$. This value is compatible with $\chi_{\mathbb{Q}}/\bar{N} \approx 1$, which was reported in the quenched lattice simulations in [44]. For comparison, we note that in the chiral soliton model, the nucleon axial singlet coupling was found to be about 0.36 [45].

In the grand canonical and unquenched QCD instanton vacuum, the topological fluctuations are substantially depleted by screening from the light quarks [18,19]:

$$\frac{\chi_{\mathbb{U}\mathbb{Q}}}{\bar{N}} = \frac{M_1^2 \langle\overline{\psi}\psi\rangle}{n_{I+\bar{I}}}\left(\frac{2N_f\langle\overline{\psi}\psi\rangle}{f_\pi^2} - M_1^2 \sum_{f=1}^{N_f} \frac{1}{m_f}\right)^{-1} \to \frac{1}{N_f}\left(\frac{f_\pi^2 M_1^2}{2n_{I+\bar{I}}}\right)\left(1 + \frac{M_1^2}{m_\pi^2}\right)^{-1} \tag{32}$$

with $m_f \to m$. The intrinsic quark spin follows from (31) with the substitution $M_1 \to m_\pi$, which is seen to vanish in the chiral limit. This null result is caused by the unpaired quark zero modes, as streamlined by the random matrix theory [46].

Since the mixing between the quark spin of the nucleon and the topological charge takes place locally in the nucleon state, we expect it to be weakly sensitive to this screening so that the quenched result (31) still holds. This observation is consistent with the large axial singlet charge reported in [47] in the canonical QCD instanton vacuum for both the quenched and unquenched ensembles.

3.4. Spin Sum Rule

The breakdown for the nucleon spin budget (17) yields the estimates ($S_N = \frac{1}{2}$):

$$\begin{aligned}\frac{\frac{1}{2}\Sigma_Q^N}{S_N} &\approx \frac{N_f}{3}\frac{\chi_{\mathbb{Q}}}{\bar{N}} \approx 60\% \\ \frac{L_Q^N}{S_N} &\approx \frac{1}{1+\kappa}\left(1-\frac{N_f}{3}\frac{\chi_{\mathbb{Q}}}{\bar{N}}\right) \approx 36\% \\ \frac{J_G^N}{S_N} &\approx \frac{\kappa}{1+\kappa}\left(1-\frac{N_f}{3}\frac{\chi_{\mathbb{Q}}}{\bar{N}}\right) \approx 4\% \end{aligned} \tag{33}$$

using the quenched topological susceptibility, with $M_u/m_N \approx 0.31 \approx 1/3$ [27] and $\kappa \equiv \pi^2\bar{\rho}^4 n_{I+\bar{I}} \approx 0.1$ at the soft renormalization scale fixed by the mean instanton density $\bar{\rho} = 0.3$ fm.

Equation (33) shows that in the QCD instanton vacuum, about 60% of the nucleon spin stems from the spin of the valence quarks as they hop and mix with the vacuum topological charge fluctuations, 36% stems from their orbital motion, and only 4% from the emerging valence gluons as the topological charge fluctuates. Our result for the intrinsic quark spin is larger than the 30–40% result reported by COMPASS [2]. Our small valence gluon contribution to the spin is comparable to the small intrinsic gluon helicity reported by COMPASS [48–50] and other collaborations.

This budgeting of the nucleon spin is to be compared with the lattice composition reported in [4], with 25% for the intrinsic quark spin, 47% for the quark orbital momentum, and 28% for the valence gluon contribution at the harder renormalization scale $\mu = 2$ GeV. More recently, lattice results were also reported in [5], with 40% for the intrinsic quark spin, 42% for the quark orbital momentum, and 27% for the valence gluon contribution, also at $\mu = 2$ GeV.

Our results at the soft renormalization scale appear to be closer to those in [5], especially with their large up-quark result of about 80%, although with a smaller valence gluon contribution. The absence of a negative down-quark contribution in our case ([5] reports -20%) follows from the quark–scalar diquark approximation in which the d-quark spin is locked. This may be improved. In addition, the quantum evolution to the harder lattice scale of $\mu = 2$ GeV will enhance the valence gluon contribution at the expense of the other contributions.

Since our results tie the intrinsic spin contribution to the quenched topological susceptibility, it would be useful for the lattice collaborations in [4,5] to report their numerical values for the topological susceptibility along with the spin budget.

4. Conclusions

The QCD instanton vacuum is populated by instantons and anti-instantons constantly tunneling between vacua with different topological charges. Their mean tunneling rate of about 1 per fm^4 sets the scale for the quantum breaking of conformal symmetry. This effect gives rise to a finite and positive gluon condensate, the primordial epoxy or hard glue at the origin of most light hadron masses.

The way a light quark can propagate coherently through this maze of tunneling configurations is through its zero mode, by locking its spin-color to zero, tunneling through an instanton and hopping to the closest anti-instanton. The tunneling through the instanton flips chirality and is at the origin of the U(1) axial anomaly and the anomalously large η' mass [22].

In a polarized proton such as a quark–diquark state, the spin of the unpaired quark is constantly in flux with the topological charge of the liquid. As a result, the intrinsic quark spin of the proton is fixed by the (quenched) vacuum topological susceptibility. A measure of the intrinsic quark spin is a measure of the (quenched) vacuum topological susceptibility.

This fundamental mechanism yields a nucleon with an intrinsic quark spin that is smaller than 1, but still larger than the one reported by the COMPASS collaboration [2]. This shortcoming may be partly fixed by relaxing the quark–diquark assumption for the nucleon, and perhaps by scale evolution.

Finally, the self-dual character of the topological gauge fields yields a small gluon contribution to the spin of the nucleon that naturally explains the null helicity polarization reported by the COMPASS [48–50], STAR [51], HERMES [52], and PHENIX [53] collaborations.

Funding: This research received no external funding.

Institutional Review Board Statement: Not applicable.

Informed Consent Statement: Not applicable.

Data Availability Statement: Not applicable.

Acknowledgments: I would like to thank Edward Shuryak, Xiang-Dong Ji, and Zein-Eddine Meziani for the discussions. This work is supported by the Office of Science, U.S. Department of Energy under Contract No. DE-FG-88ER40388.

Conflicts of Interest: The author declares no conflict of interest.

Appendix A. Measuring the QCD Vacuum Topological Susceptibility

The cooled Yang-Mills vacuum in Figure 1 is composed of active topological charges that constantly flip the helicity of light quarks. The fluctuations in the topological charge add or remove from the intrinsic quark spin of the nucleon. This strategic relationship is mediated by the U(1) anomaly and is best captured by recasting the result (31) in the more generic form:

$$\Sigma_Q^N \approx \frac{N_f}{3}\frac{\chi_{\mathbb{Q}}}{\bar{N}} \approx \frac{N_F}{96\pi^2}\int d^4x \frac{\langle F\tilde{F}(x)\, F\tilde{F}(0)\rangle_{\mathbb{Q}}}{\langle F^2(0)\rangle} \tag{A1}$$

with the estimate $M_u(0)/m_N \approx 1/3$. A measure of the quark spin contribution in the proton (on the left-hand side) is a measure of the QCD vacuum susceptibility normalized to the mean topological density (on the right-hand side). Since (A1) is a polarized nucleon-connected matrix element, it is natural that it probes the fluctuations of $F\tilde{F}$ in the Yang-Mills vacuum.

References

1. Ashman, J.; Badelek, B.; Baum, G.; Beaufays, J.; Bee, C.P.; Benchouk, C.; Bird, I.G.; Brown, S.C.; Caputo, M.C.; Cheung, H.W.K. A Measurement of the Spin Asymmetry and Determination of the Structure Function g(1) in Deep Inelastic Muon-Proton Scattering. *Phys. Lett. B* **1988**, *206*, 364. [CrossRef]
2. Adolph, C. The spin structure function gp 1 of the proton and a test of the Bjorken sum rule. *Phys. Lett. B* **2016**, *753*, 18–28. [CrossRef]
3. Gabathuler, E. Where is the nucleon spin? *Nat. Phys.* **2006**, *2*, 303–304. [CrossRef]
4. Yang, Y.; Liang, J.; Bi, Y.; Chen, Y.; Draper, T.; Liu, K.; Liu, Z. Proton Mass Decomposition from the QCD Energy Momentum Tensor. *Phys. Rev. Lett.* **2018**, *121*, 212001. [CrossRef] [PubMed]
5. Alexandrou, C.; Constantinou, M.; Hadjiyiannakou, K.; Jansen, K.; Kallidonis, C.; Koutsou, G.; Avilés-Casco, A.V.; Wiese, C. Nucleon Spin and Momentum Decomposition Using Lattice QCD Simulations. *Phys. Rev. Lett.* **2017**, *119*, 142002. [CrossRef]
6. Ji, X.; Yuan, F.; Zhao, Y. What we know and what we don't know about the proton spin after 30 years. *Nat. Rev. Phys.* **2021**, *3*, 27–38. [CrossRef]
7. Diakonov, D. Chiral symmetry breaking by instantons. *Proc. Int. Sch. Phys. Fermi* **1996**, *130*, 397–432.
8. Schäfer, T.; Shuryak, E.V. Instantons in QCD. *Rev. Mod. Phys.* **1998**, *70*, 323–426. [CrossRef]
9. Nowak, M.A.; Rho, M.; Zahed, I. *Chiral Nuclear Dynamics*; World Scientific: Singapore, 1996.
10. Ji, X. Gauge-Invariant Decomposition of Nucleon Spin. *Phys. Rev. Lett.* **1997**, *78*, 610–613. [CrossRef]
11. Biddle, J.C.; Kamleh, W.; Leinweber, D.B. Visualization of center vortex structure. *Phys. Rev. D* **2020**, *102*, 034504. [CrossRef]
12. Biddle, J.C.; Kamleh, W.; Leinweber, D.B. Visualisations of Centre Vortices. *EPJ Web Conf.* **2020**, *245*, 06010. [CrossRef]
13. Leinweber, D.B. Visualizations of the QCD vacuum. In Proceedings of the Workshop on Light-Cone QCD and Nonperturbative Hadron Physics, Adelaide, Australia, 13–22 December 1999; pp. 138–143.
14. Shuryak, E.V. The Role of Instantons in Quantum Chromodynamics. 1. Physical Vacuum. *Nucl. Phys. B* **1982**, *203*, 93. [CrossRef]
15. Chu, M.C.; Grandy, J.M.; Huang, S.; Negele, J.W. Correlation functions of hadron currents in the QCD vacuum calculated in lattice QCD. *Phys. Rev. D* **1993**, *48*, 3340–3353. [CrossRef] [PubMed]
16. Ji, X.; Liu, Y. Quantum Anomalous Energy Effects on the Nucleon Mass. *arXiv* **2021**, arXiv:2101.04483.

17. Novikov, V.A.; Shifman, M.A.; Vainshtein, A.I.; Zakharov, V.I. Are All Hadrons Alike? *Nucl. Phys. B* **1981**, *191*, 301–369 [CrossRef]
18. Diakonov, D.; Polyakov, M.V.; Weiss, C. Hadronic matrix elements of gluon operators in the instanton vacuum. *Nucl. Phys. B* **1996**, *461*, 539–580. [CrossRef]
19. Kacir, M.; Prakash, M.; Zahed, I. Hadrons and QCD instantons: A Bosonized view. *Acta Phys. Polon. B* **1999**, *30*, 287–348.
20. Witten, E. Current Algebra Theorems for the U(1) Goldstone Boson. *Nucl. Phys. B* **1979**, *156*, 269–283. [CrossRef]
21. Veneziano, G. U(1) Without Instantons. *Nucl. Phys. B* **1979**, *159*, 213–224. [CrossRef]
22. t Hooft, G. Computation of the Quantum Effects Due to a Four-Dimensional Pseudoparticle. *Phys. Rev. D* **1976**, *14*, 3432–3450. [CrossRef]
23. Verbaarschot, J.J.M.; Zahed, I. Spectral density of the QCD Dirac operator near zero virtuality. *Phys. Rev. Lett.* **1993**, *70*, 3852–3855. [CrossRef] [PubMed]
24. Wittig, H. QCD on the Lattice. In *Particle Physics Reference Library: Volume 1: Theory and Experiments*; Schopper, H., Ed.; Springer: Cham, Switzerland, 2020; pp. 137–262.
25. Pobylitsa, P.V. The Quark Propagator and Correlation Functions in the Instanton Vacuum. *Phys. Lett. B* **1989**, *226*, 387–392. [CrossRef]
26. Kock, A.; Liu, Y.; Zahed, I. Pion and kaon parton distributions in the QCD instanton vacuum. *Phys. Rev. D* **2020**, *102*, 014039. [CrossRef]
27. Schäfer, T.; Shuryak, E.V.; Verbaarschot, J.J.M. Baryonic correlators in the random instanton vacuum. *Nucl. Phys. B* **1994**, *412*, 143–168. [CrossRef]
28. Bernard, V.; Meissner, U.G.; Zahed, I. Decoupling of the Pion at Finite Temperature and Density. *Phys. Rev. D* **1987**, *36*, 819. [CrossRef] [PubMed]
29. Klevansky, S.P. The Nambu-Jona-Lasinio model of quantum chromodynamics. *Rev. Mod. Phys.* **1992**, *64*, 649–708. [CrossRef]
30. Roberts, C.D.; Richards, D.G.; Horn, T.; Chang, L. Insights into the Emergence of Mass from Studies of Pion and Kaon Structure. *arXiv* **2021**, arXiv:2102.01765.
31. Diakonov, D.; Maul, M. Center vortex solutions of the Yang-Mills effective action in three and four dimensions. *Phys. Rev. D* **2002**, *66*, 096004. [CrossRef]
32. Diakonov, D.; Petrov, V.Y.; Pobylitsa, P.V. The Wilson Loop and Heavy Quark Potential in the Instanton Vacuum. *Phys. Lett. B* **1989**, *226*, 372–376. [CrossRef]
33. Greensite, J. Confinement from Center Vortices: A review of old and new results. *EPJ Web Conf.* **2017**, *137*, 01009. [CrossRef]
34. Karsch, F. Deconfinement and chiral symmetry restoration. In Proceedings of the 3rd International Con- ference on Strong and Electroweak Matter, Copenhagen, Denmark, 2–5 December 1998; pp. 101–111.
35. Altarelli, G.; Ross, G.G. The Anomalous Gluon Contribution to Polarized Leptoproduction. *Phys. Lett. B* **1988**, *212*, 391–396. [CrossRef]
36. Carlitz, R.D.; Collins, J.C.; Mueller, A.H. The Role of the Axial Anomaly in Measuring Spin Dependent Parton Distributions. *Phys. Lett. B* **1988**, *214*, 229–236. [CrossRef]
37. Hatsuda, T.; Zahed, I. The Spin of the Proton and the Axial Anomaly. *Phys. Lett. B* **1989**, *221*, 173–176. [CrossRef]
38. Ji, X. U(1) axial charge in the chiral limit. *Phys. Rev. Lett.* **1990**, *65*, 408–411. [CrossRef]
39. Tarasov, A.; Venugopalan, R. The role of the chiral anomaly in polarized deeply inelastic scattering I: Finding the triangle graph inside the box diagram in Bjorken and Regge asymptotics. *Phys. Rev. D* **2020**, *102*, 114022. [CrossRef]
40. Narison, S.; Shore, G.M.; Veneziano, G. Target independence of the EMC-SMC effect. *Nucl. Phys. B* **1995**, *433*, 209–233. [CrossRef]
41. Kuhn, J.H.; Zakharov, V.I. Towards universality of the isosinglet axial coupling. *Phys. Lett. B* **1990**, *252*, 615–619. [CrossRef]
42. Forte, S.; Shuryak, E.V. Instanton induced suppression of the singlet axial charge of the proton. *Nucl. Phys. B* **1991**, *357*, 153–166. [CrossRef]
43. Anselm, A. Isosinglet axial coupling and the number of instantons inside the proton. *Phys. Lett. B* **1992**, *291*, 455–458. [CrossRef]
44. Luscher, M.; Palombi, F. Universality of the topological susceptibility in the SU(3) gauge theory. *JHEP* **2010**, *09*, 110. [CrossRef]
45. Blotz, A.; Polyakov, M.V.; Goeke, K. The Spin of the proton in the solitonic SU(3) NJL model. *Phys. Lett. B* **1993**, *302*, 151–156. [CrossRef]
46. Janik, R.A.; Nowak, M.A.; Papp, G.; Zahed, I. The U(1) problem in chiral random matrix models. *Nucl. Phys. B* **1997**, *498*, 313–330. [CrossRef]
47. Schäfer, T.; Zetocha, V. Instantons and the spin of the nucleon. *Phys. Rev. D* **2004**, *69*, 094028. [CrossRef]
48. Ageev, E.S.; Alexakhin, V.Y.; Alexandrov, Y.; Alexeev, G.D.; Amoroso, A.; Badelek, B.; Balestra, F.; Ball, J.; Baum, G.; Bedfer, Y.; et al. Gluon polarization in the nucleon from quasi-real photoproduction of high-p(T) hadron pairs. *Phys. Lett. B* **2006**, *633*, 25–32. [CrossRef]
49. Stolarski, M.; COMPASS Collaboration. The COMPASS results on longitudinal spin effects and future measurements. *Nucl. Phys. B Proc. Suppl.* **2010**, *207–208*, 53–56. [CrossRef]
50. Adolph, C.; Alekseev, M.G.; Alexakhin, V.Y.; Alexandrov, Y.; Alexeev, G.D.; Amoroso, A.; Antonov, A.A.; Austregesilo, A.; Badelek, B.; Balestra, F.; et al. Leading and Next-to-Leading Order Gluon Polarization in the Nucleon and Longitudinal Double Spin Asymmetries from Open Charm Muoproduction. *Phys. Rev. D* **2013**, *87*, 052018. [CrossRef]
51. Djawotho, P. Gluon polarization and jet production at STAR. *J. Phys. Conf. Ser.* **2011**, *295*, 012061. [CrossRef]

52. Airapetian, A.; Akopov, N.; Akopov, Z.; Aschenauer, E.C.; Augustyniak, W.; Avakian, R.; Avetissian, A.; Avetisyan, E.; Belostotski, S.; Bianchi, N.; et al. Leading-Order Determination of the Gluon Polarization from high-p(T) Hadron Electroproduction. *JHEP* **2010**, *8*, 130. [CrossRef]
53. Adare, A.; Bickley, A.A.; Ellinghaus, F.; Glenn, A.; Kinney, E.; Nagle, J.L.; Seele, J.; Wysocki, M.; Afanasiev, S.; Isupov, A.; et al. Inclusive cross section and double helicity asymmetry for pi^0 production in p^+p collisions at $\sqrt{s} = 62.4$ GeV. *Phys. Rev. D* **2009**, *79*, 012003. [CrossRef]